fibers

MDPI

Article

Facile Fabrication of PA66/GO/MWNTs-COOH Nanocomposites and Their Fibers

Xuefeng Gao [1,2,3], Wenguang Yu [1,2,3], Xianye Zhang [1,2,3], Jiao Zhang [1,2,3], Haihui Liu [1,2,3] and Xingxiang Zhang [1,2,3,*]

1 Tianjin Municipal Key Laboratory of Advanced Fiber and Energy Storage, School of Material Science and Engineering, Tianjin Polytechnic University, Tianjin 300387, China
2 Advanced Textile and Composite Key Lab of the Ministry of Education, School of Material Science and Engineering, Tianjin Polytechnic University, Tianjin 300387, China
3 School of Material Science and Engineering, Tianjin Polytechnic University, Tianjin 300387, China
* Correspondence: zhangpolyu@aliyun.com

Received: 20 June 2019; Accepted: 23 July 2019; Published: 25 July 2019

Abstract: Good dispersion and interfacial compatibility are the key issues to realize the full potential of the physical–mechanical properties of nanocarbon-materials reinforced composites. Styrene–maleic-anhydride-copolymer (SMA)-treated graphene oxide (GO), carboxylated multiwalled carbon nanotubes (MWNTs-COOH), and solid-state shear milling (S3M) were applied to further improve the physical–mechanical properties of the nanocomposite fibers. The results show that a mixture of GO/MWNTs-COOH exhibits good dispersion and interfacial compatibility in polyamide-66 (PA66) matrix. Consequently, the physical–mechanical properties of the fibers, which were spun from the nanocomposite of GO/MWNTs-COOH treated using SMA and S3M methods, show a significant enhancement compared to the untreated fibers as well as better crystallization and thermal properties. In particular, the tensile strength of the PA66/GO/MWNTs-COOH nanocomposite fibers with a loading of 0.3 wt % GO/MWNTs-COOH reaches a maximum (979 MPa), which is the highest among all of the reported literature values. Moreover, the fibers were fabricated by a facile process with efficiency, holding great potential for industrial applications.

Keywords: nanocomposite fiber; graphene oxide; multi-walled carbon nanotubes; solid-state shear milling; styrene–maleic anhydride copolymer

1. Introduction

Polyamide 66 (PA66) has been widely used due to excellent mechanical properties, high thermal stability, processability, and relatively low cost. However, its applications, such as its use in tire cord and conveyor belts, are limited because of insufficient strength. To further improve the physical–mechanical properties of PA66, many additives have been used in the research, such as glass fiber [1,2], carbon fiber [3], carbon nanotubes [4–8], graphene [9], and so forth [10–14].

Composite materials with graphene and carbon nanotube additives have long been considered as exciting prospects among nanotechnology applications. In order to improve physical–mechanical and electrical properties, many researchers have paid more attention to the graphene- and carbon-nanotube-reinforced polymers [15–18]. The improvement of physical–mechanical properties of the nanocomposite materials is expected to fill the gap in the performance and price between carbon-fiber- and glass-fiber-reinforced resin composites [19]. However, graphene oxide (GO) and multiwalled carbon nanotubes (MWNTs) are difficult to disperse uniformly in polymer matrix due to their large specific surface area and ratio of length/diameter, high surface energy, and strong π-π conjugate forces, which make them stack and entangle to an extreme degree. Additionally, the weak surface binding energy

between polymer and GO or MWNTs makes it hard to transfer force from polymer to GO or MWNTs, which leads to GO/MWNTs being pulled out under shear stress [20]. The homogeneous dispersion and interfacial compatibility of GO and MWNTs within the polymer matrix are the key challenges in improving the strength of composites. Many methods have been tested, such as melting blended [21,22], solution blended [23], and in situ polymerization [4,5] methods. Noncovalent functional [24,25] and covalent functional [4,5] MWNTs have been used to enhance the binding energy. However, little research has been reported about how to disperse carbon materials inside the polymer composite in a facile, low cost, and quick way, which considerably hinders its industrial application.

Many studies have confirmed that direct melt blending is not an efficient method for the satisfactory dispersion quality and properties of the resultant polymer/carbon material composites. The milling technique has been applied to treat carbon materials in order to prepare nanocomposites [26,27]. The S3M process has been used to realize the exfoliation of layered fillers [28] and the cutting and dispersion of CNTs [29] in polymer composites. In this work, we aim to study a facile mass production method for nanocomposite fibers with excellent thermal and physical–mechanical properties.

A synergistic reinforcement was shown in the styrene–maleic anhydride copolymer (SMA) grafted GO/MWNT/Polyamide 6 nanocomposite fiber with a total loading of 0.5 wt % [30], however, a grafted polymerization process was necessary prior to in situ polymerization. In this study, GO and MWNTs-COOH were mixed at a mass ratio of 2:3. First, we treated GO/MWNTs-COOH using sodium salt of SMA by ultrasonication, which is beneficial to improve the interfacial adhesion of carbon materials and the compatibility with matrix [30–32]. Then, the PA66/GO/MWNTs-COOH nanocomposites were fabricated by the S3M process. The resultants were melt-spun into fibers and further stretched. Both the thermal and mechanical properties of the nanocomposite fibers were then investigated.

2. Materials and Methods

2.1. Materials

PA66 (EPR27) was obtained from Pingdingshan Shenma Co., Ltd, China, with a melt index of 10.8 g/10 min and a relative viscosity of 2.67. GO (a lateral size of 3–7 μm, layer number <5) was supplied as a bulk, dry powder by Changzhou Sixth Element Co., Ltd., China. MWNTs-COOH (diameter <8 nm, lengths 0.5–2 μm) were supplied by Beijing Deke Daojin Co., Ltd., China. An emulsion of sodium salt of SMA (2.5 wt %) was obtained from Shanghai Leather Chemical Factory. Sulfuric acid (H_2SO_4) was supplied by Tianjin Kermel Reagents Co., Ltd., China.

2.2. Fabrication of the SMA-Treated Mixture of GO/MWNTs-COOH

GO (2 g) and MWNTs-COOH (3 g) powder were added to SMA aqueous solution (200 g) to obtain a uniformly dispersed suspension, sonicated at 50 °C for 4 h. The suspension was separated by filtration. The black solid was dried by an air-circulating oven at 25 °C for 24 h. The black powder, with a mass ratio of 2:3 between GO and MWNTs-COOH, was obtained by grinding.

2.3. Fabrication of the PA66/GO/MWNTs-COOH Nanocomposite Chips

PA66 chips were first dried by using an oven at 130 °C for 10 h. Then, PA66 chips and 5 wt % GO/MWNTS-COOH mixtures were fed into self-designed S3M equipment with a rotation rate of 525 rpm. It took 5 min to complete a whole cycle of milling 5 kg of the mixture of PA66 and GO/MWNT-COOH. A fine compounding powder of PA66 and 5 wt % GO/MWNTs-COOH can be obtained by milling five cycles. By diluting the compounding powder with pure PA66 through a melting process (two-rotor continuous extrusion processing at 280 °C), the PA66/GO/MWNTs-COOH nanocomposites (with various loading of GO/MWNTs-COOH: 0.1, 0.2, 0.3, 0.4, and 0.5 wt %) were fabricated. The same extrusion process was used in the conventional blending nanocomposites, in which the same GO/MWNTs-COOH loadings with pure PA66 chips were mixed without the S3M process.

2.4. Fabrication of the PA66/GO/MWNTs-COOH Nanocomposite Fibers

All the chips were dried and tumbled in a drum dryer to remove moisture at 130 °C for 24 h under vacuum. By doing so, the moisture on the surface of the chip was less than 50 ppm, which was measured by a Karl Fischer moisture meter. Figure 1 shows the fabrication of the nanocomposite and the melt spinning process. Chips were melted at 290 °C and then extruded with a multifilament spinneret (24 holes) with a diameter of 0.3 mm. First, the primary fiber was stretched five times using the rapid drawing process, and four godet rollers were used (GR 1: 85 °C, 70 m/min; GR 2: 170 °C, 280 m/min; GR 3: 210 °C, 350 m/min; GR 4: 80 °C, 350 m/min). Then, the obtained fiber was further stretched 1.2 times to its final length by the slow drawing process, and three sets of godet rollers were used (GR 5: 70 °C, 20 m/min; GR 6: 150 °C, 23 m/min; GR 7: 200 °C, 24 m/min). The draw ratio between the first godet roller (GR 1) and the final godet roller (GR 7) was 6, with the final yarn specification being 125 dtex/24 filaments.

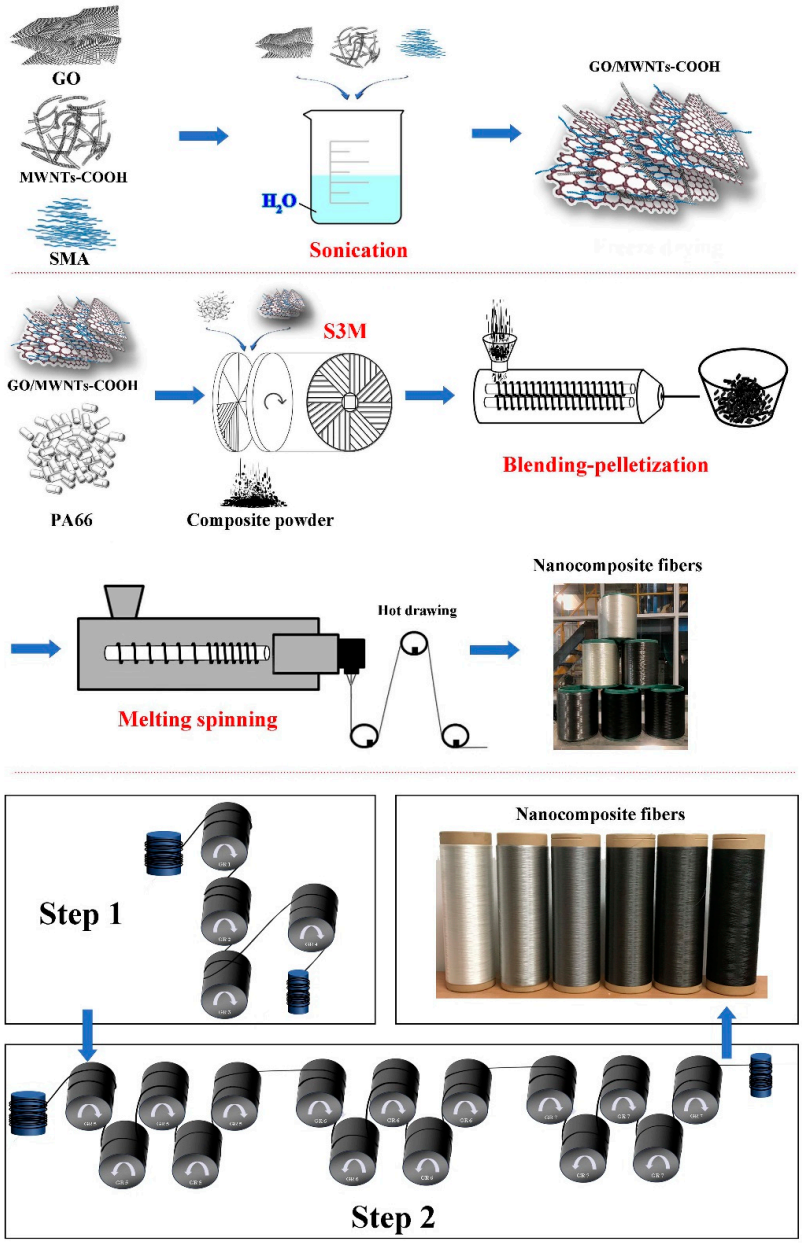

Figure 1. Schematic diagram of fabrication of polyamide 66 (PA66)/graphene oxide (GO)/carboxylated multiwalled carbon nanotubes (MWNTs-COOH) nanocomposite fibers.

2.5. Characterization

Fourier-transform infrared (FTIR) spectra of the samples were identified by a spectrometer (Bruker TERSOR37, Karlsruhe, Germany) in the range of 4000–400 cm^{-1}. The nanocomposite fibers were characterized by a field-emission scanning electron microscope (FE-SEM, Hitachi S-4800, Tokyo, Japan). The microstructures of the nanocomposite fibers were observed using a transmission electron microscope (TEM, Hitachi H-7650, Tokyo, Japan) operating at an accelerating voltage of 100 kV. The thermal properties of 5–10 mg samples were identified using a differential scanning calorimeter (DSC, Netzsch 204 F1, Bavaria, Germany). DSC scans were performed from 30 to 300 °C with a rate of ±10 °C/min in a heating–cooling–heating cycle in N_2 atmosphere. A STA409PC system from NETZSCH (Bavaria, Germany) was used to test thermogravimetric analysis (TGA) and derivative thermogravimetry (DTG) under a flowing nitrogen atmosphere, where samples (5–10 mg) were heated from 40 to 800 °C at a heating rate of 10 °C/min. A dynamic mechanical analyzer (NETZSCH DMA 242E, Bavaria, Germany) was used to measure the glass-transition temperature (T_g) of the nanocomposite fibers at a vibration frequency of 1 Hz and scanning temperature range from 30 °C to 120 °C at a heating rate of 3 °C/min. A diffractometer (Rigaku D/MAX-gA, Tokyo, Japan) with filtered Cu Kα radiation (λ = 0.15406 nm) was used for X-ray diffraction (XRD) in a range from 3° to 40° (2θ) and a scan rate of 8°/min at room temperature. An optical microscope (OM, OLYMPUS-BX51, Tokyo, Japan) was used to characterize the dispersibility and secondary agglomeration of GO/MWNTs-COOH in the PA66/GO/MWNTs-COOH nanocomposite fiber with various GO/MWNTs-COOH loadings. A fiber tensile tester (ZS408, Huaxin, China) was used to test the physical–mechanical properties of the PA66/GO/MWNTs-COOH nanocomposite fibers with a test length of 200 mm at a rate of 200 mm/min for 10 times.

The molecular weight of the pure PA66 and the nanocomposites chips were calculated from the Mark–Houwink Equation (1):

$$[\eta] = \mathrm{K} \times M^{\alpha}, \quad (1)$$

where M is the average molecular weight and $[\eta]$ is the intrinsic viscosity ($\mathrm{K} = 3.93 \times 10^{-2}$ mL/g, $\alpha = 0.78$). $[\eta]$ was measured at a concentration of 0.01 g/mL in H_2SO_4 with a flexible system (AVS 370, Julabo, Bavaria, Germany) at 20 °C. The relative viscosity (η_r) of samples was measured three times.

3. Results and Discussion

3.1. FTIR Analysis

The FTIR spectra of the GO, MWNTs-COOH, and GO/MWNT-COOH powders are presented in Figure 2. Characteristic GO bands appear at 1730 cm^{-1} (C=O stretching), 1385 cm^{-1} (C$[\eta] = \mathrm{K} \times M^{\alpha}$OH stretching), and 1041 cm^{-1} (C$[\eta] = \mathrm{K} \times M^{\alpha}$O of epoxy stretching). Characteristic MWNTs-COOH bands appear at 1710 cm^{-1} (stretching vibrations of carboxyl groups) and 1105 cm^{-1} (C$[\eta] = \mathrm{K} \times M^{\alpha}$O stretching vibrations). The SMA-treated GO/MWNT-COOH shows all the characteristic peaks of GO and MWNTs-COOH.

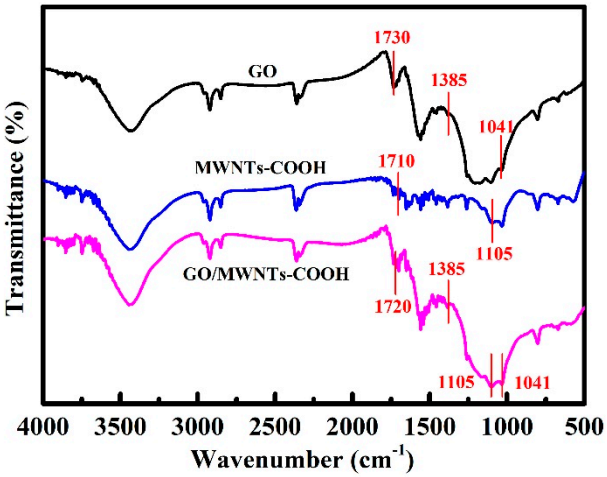

Figure 2. FTIR spectra of GO, MWNTs-COOH, and GO/MWNT-COOH.

3.2. Viscosity Analysis

In order to assess the impact of the loaded GO/MWNTs-COOH on the molecular weight of PA66, the molecular weight of PA66 and GO/MWNTs-COOH/PA66 was determined through relative viscosity measurements, as shown in Table 1. It can be seen that the relative viscosity of PA66 with the GO/MWNTs-COOH loading increases first and then decreases. As the incorporation of GO/MWNTs-COOH increased, the relative viscosity of GO/MWNTs-COOH/PA66 increased from 2.64 to 2.86 when 0.3 wt % GO/MWNTs-COOH was loaded. This phenomenon can be described as follows: When the loading of GO/MWNTs-COOH is low, it can be uniformly dispersed in the PA66 matrix, which restrains the movement of PA66 chains and causes the fluidity to deteriorate, thereby increasing the viscosity. When the load is further increased, GO and MWNTs-COOH agglomerate, and the hindrance to the PA66 molecular chain is reduced–the fluidity is improved and the viscosity is lowered.

Table 1. Molecular weight and viscosity of pure and nanocomposite chips.

Sample	Time (s)	$[\eta_r]$ [1]	$[\eta_{sp}]$ [2]	$[\eta]$ [3]	M [4]
H_2SO_4	136.14	1	0	0	-
a	370.15	2.64	1.6377	115.57	27,972
b	383.26	2.82	1.8152	124.91	30,903
c	386.73	2.84	1.8407	126.23	31,323
d	388.97	2.86	1.8571	127.07	31,590
e	383.26	2.82	1.8152	124.91	30,903
f	379.55	2.79	1.7879	123.50	30,457

Note: (a) PA66; (b) 0.1 wt % GO/MWNTs-COOH; (c) 0.2 wt % GO/MWNTs-COOH; (d) 0.3 wt % GO/MWNTs-COOH; (e) 0.4 wt % GO/MWNTs-COOH; and (f) 0.5 wt % GO/MWNTs-COOH; [1] Relative viscosity; [2] specific viscosity; [3] intrinsic viscosity; and [4] molecular weight.

3.3. Morphology and Structure of GO/MWNTs-COOH and Nanocomposite Fibers

TEM micrographs of GO, MWNTs-COOH, and their mixtures are shown in Figure 3. Compared with pure GO and MWNTs-COOH, the mixture shows MWNTs-COOH inserting into the layers of GO, which is obtained using the SMA-treatment, thus reducing the stacking of GO and the agglomeration of MWNTs-COOH. Many folds can be observed on the surface of GO. These folds provide a better interface with the matrix, providing better stress transfer in the matrix. This result is advantageous for enhancing the binding between GO/MWNTs-COOH and PA66 and for improving the mechanical properties of the fiber.

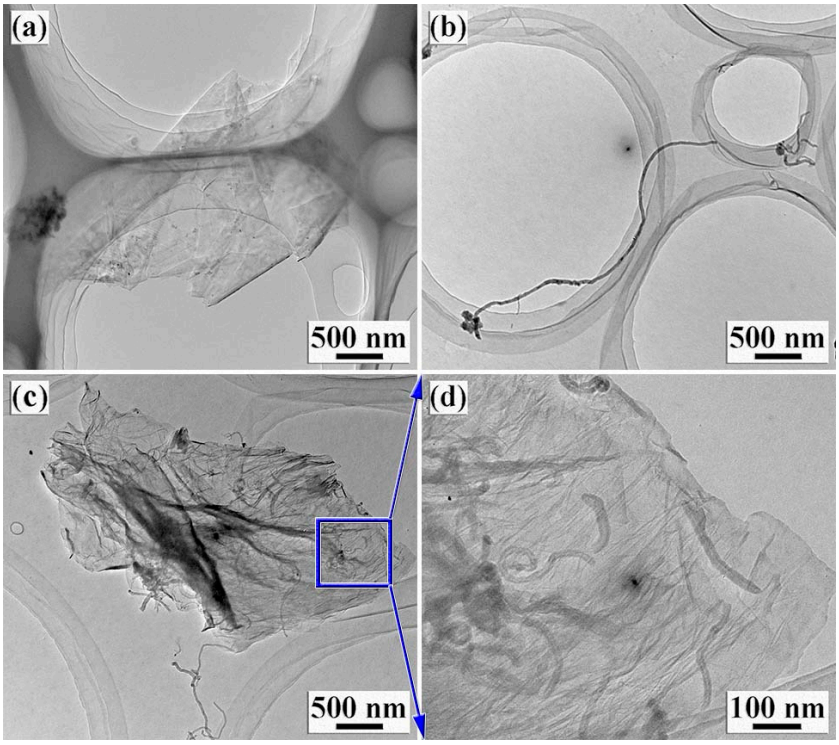

Figure 3. TEM micrographs: (**a**) GO; (**b**) MWNTs-COOH; and (**c,d**) GO and MWNTs-COOH mixture at 500 and 100 nm, respectively.

Solving the agglomeration problem of GO/MWNTs-COOH and ensuring the homogeneous dispersion of GO/MWNTs-COOH along the nanocomposite fibers' axes in polymer matrices are the key to improve the mechanical performance of the nanocomposite fibers. Figure 4a–d are SEM images of the surface and the fracture surface of pure PA66 and nanocomposite fibers. The GO and MWNTs-COOH are evenly dispersed, both GO and MWNTs-COOH are apt to adhere on PA66 chains for effectively transferring the stress on the matrix to GO and MWNTs-COOH, leading to GO/MWNTs- COOH resisting to be pulled out from the matrix. Thereby, it is hoped that the physical–mechanical properties of the nanocomposite fibers are effectively improved. The morphology of the nanocomposite fibers was observed by OM, in which the dispersion of dark spots is the GO/MWNTs-COOH, consistent with the SEM microimages. Moreover, the GO/MWNTs-COOH without agglomeration dispersed homogeneously in polymer matrices along the nanocomposite fiber's axis can be observed in Figure 4f. The orientation of GO/MWNTs-COOH along the drawing direction is crucial for the mechanical performance of the nanocomposites [33]. Therefore, the SEM and OM micrograph results indicate that the nanocomposite fibers with 0.3 wt % of GO/MWNTs-COOH have a better mechanical performance.

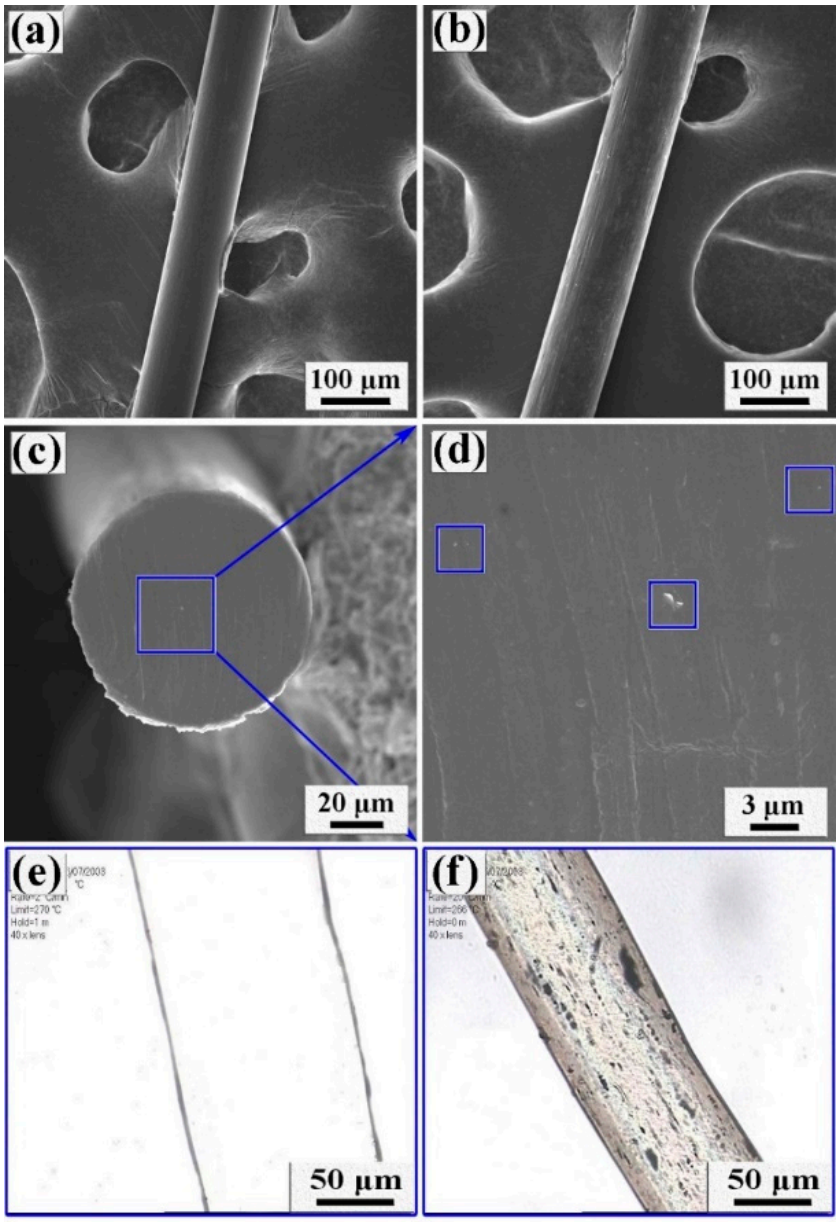

Figure 4. SEM micrographs of the surface and fracture surface of nanocomposite fibers ((**a**), pure PA66; (**b**)–(**d**(, 0.3 wt % at 100, 20, and 3 µm, respectively); OM micrographs of pure and nanocomposite fibers ((**e**), pure PA66; (**f**), 0.3 wt %).

3.4. Physical–Mechanical Properties

Figure 5 and Table 2 show the physical–mechanical properties of the nanocomposite fibers. Due to the even distribution of GO/MWNTs-COOH within the polymer matrix, and due to interfacial interaction [34], it is obvious that the mechanical behavior of the nanocomposite fiber with GO/MWNTs-COOH in a polymer matrix is enhanced. The tensile strength of 0.3 wt % GO/MWNTs-COOH nanocomposite fiber with S3M process is 979 MPa, which is an improvement of 32% compared to a pure PA66 fiber. The stress fiber tends to increase with lower loading, and elongation remains constant. When GO/MWNTs-COOH loading further increases, from 0.3 wt % to 0.5 wt %, the tensile strength decreases from 979 to 766 MPa. The physical–mechanical properties of the nanocomposite fibers without the S3M decrease after an initial increase. However, the performance of the fiber without the S3M process is much less than that of the fiber with the S3M process. It can be proved that the S3M process makes GO/MWNTs-COOH disperse evenly in PA66. With

increased GO/MWNTs-COOH loadings in PA66, a reassembly occurs due to van der Waals forces interacting between nanosheets. Due to the agglomerated GO/MWNTs-COOH, the physical–mechanical properties of the nanocomposite fibers decrease, resulting in stress concentration. With increasing GO/MWNTs-COOH loadings, the Young's modulus of the nanocomposite fibers gradually increases compared to the pure fiber. Until 0.5 wt % GO/MWNTs-COOH loading, Young's modulus is improved by about 41% compared to the pure fiber. The reason may be attributed to the interaction between GO/MWNTs-COOH and the PA66, which limits the motion of the PA66 chains. With increasing GO/MWNTs-COOH loading, the elongation of the nanocomposite fibers is almost constant. Compared to the S3M-untreated samples, the S3M-treated samples have better physical–mechanical properties at the same GO/MWNTs-COOH loading. This indicates that the S3M process can improve the polymer performance. Since the crystallization and orientation of the fiber were further improved by the two-step drawing process, better physical–mechanical properties can be obtained. According to PA66 fibers reinforced by graphene, carbon nanotubes, and other additives [4,21,35,36], our work has the highest physical–mechanical properties among all of the reported values.

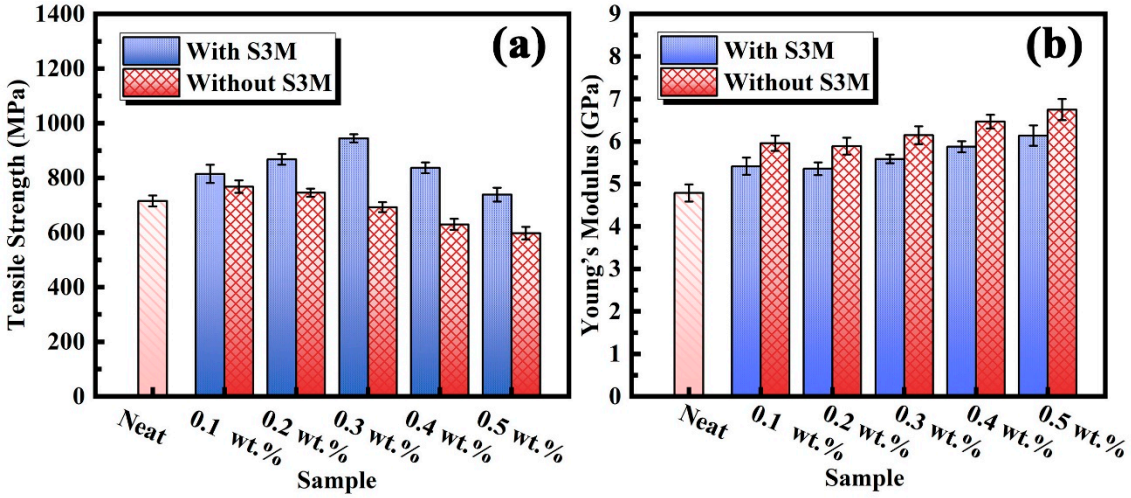

Figure 5. Physical–mechanical properties of the pure and the nanocomposite fibers: (**a**) Tensile strength and (**b**) Young's modulus.

Table 2. Physical–mechanical properties of the pure and the nanocomposite fibers.

Simple	Loadings (wt %)	Tensile Strength (MPa) (Improvement %)		Young's Modulus (GPa) (Improvement %)		Elongation (%)	Reference
		With S3M	Without S3M	With S3M	Without S3M		
PA66	0	742	742	4.96	4.96	13	This work
PA66/GO/MWNTs-COOH	0.1	845(14)	796(7)	6.18(25)	5.14(4)	12	
	0.2	899(21)	773(4)	6.10(23)	5.33(7)	11	
	0.3	979(32)	718(-3)	6.37(28)	5.35(8)	12	
	0.4	867(17)	652(-12)	6.71(35)	5.61(13)	14	
	0.5	766(3)	620(-16)	7.00(41)	5.73(16)	13	
PA66/MWNTs	0.5	-	640	-	3.05	57	[4]
PA66/MWNTs	1	-	640	-	3.78	44	[21]
PA66/MWNTs-SDBS	0.1	-	101	-	0.3	30	[35]
PA66/MWNTs-COOH	0.1	-	96	-	0.4	23	
PA66/MWNTs	1	-	96	-	4.7	150	[36]

3.5. Thermal and Crystallization Behavior

TGA and DTG tests were conducted for the pure and the nanocomposite fibers. The mass loss, due to degradation volatilization, was monitored as a function of temperature, as shown in Figure 6, corresponding to a 5% mass loss ($T_{5\ wt\ \%}$). The temperatures at the maximum rate of mass loss are

summarized in Table 3. With GO/MWNTs-COOH additions increasing, the thermal stability of the nanocomposite fibers was improved first and then reduced. Here, T_{max} is the temperature at the maximum mass loss rate regarded as the decomposition temperature. T_{max} of the nanocomposite fiber with 0.3 wt % GO/MWNTs-COOH loading is 445.2 °C, which is higher than that of the pure fiber (439.4 °C). The T_{max} improvement of the nanocomposite fiber is ascribed to the compatibility of GO/MWNTs-COOH and the PA66 matrix, which makes heat transfer fast and improves the heat resistance of the nanocomposite fiber.

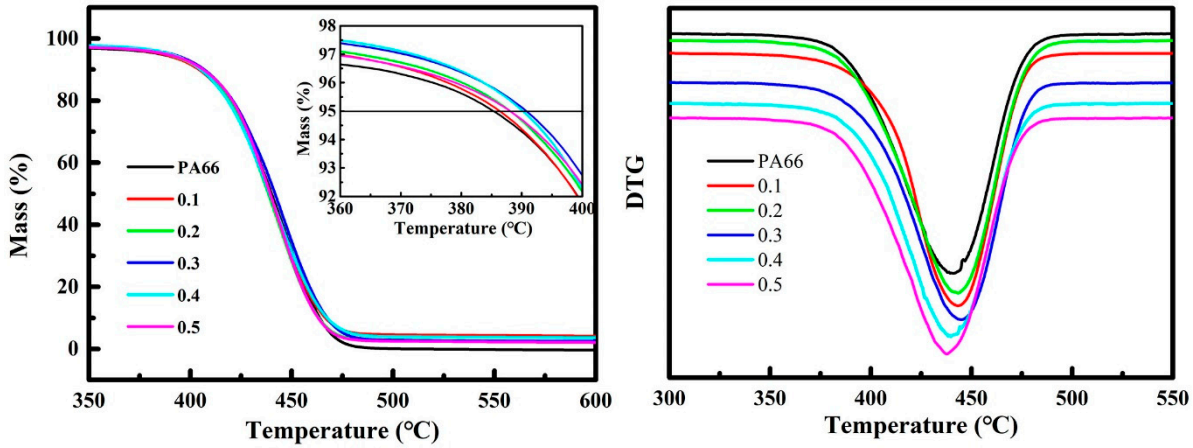

Figure 6. Thermogravimetric analysis (TGA) and DTG curves of the pure and the nanocomposite fibers.

Table 3. TGA parameters of the pure and the nanocomposite fibers.

Loadings (wt %)	$T_{5\ wt\ \%}$ (°C)	T_{max} (°C)
0	385.1	439.4
0.1	386.1	441.4
0.2	387.9	443.6
0.3	390.8	445.2
0.4	390.3	439.7
0.5	387.8	437.9

The DSC results of the pure and the nanocomposite fibers with various GO/MWNTs-COOH loadings are shown in Figure 7. Compared with the pure PA66 fibers, T_m of the nanocomposite fibers increases first and then decreases. This is explained by the GO/MWNTs-COOH and PA66 that disperse evenly and form strong interfacial interactions, resulting in a more rapid heat transfer by SMA treatment and the S3M process. Upon further increasing the GO/MWNTs-COOH loading, reassembling causes T_m to decrease.

The crystallization temperature (T_c) can be determined by analyzing cooling scans. Compared with the pure PA66 fibers, T_c of the nanocomposite fibers with 0.3 wt % GO/MWNTs-COOH loading increases by 7.2 °C due to the heterogeneous nucleating action of GO/MWNTs-COOH. The GO/MWNTs-COOH loading can improve the crystallization rate by reducing the formation power of a new crystal plane. The degree of crystallinity (X_c) values, calculated with various GO/MWNTs-COOH loadings from the normalized heat of fusion of the DSC, are listed in Table 4. The maximum crystallinity appears at 0.3 wt % GO/MWNTs-COOH loading, which is higher than that of the pure PA66 fiber. When further increasing the GO/MWNTs-COOH loading, GO/MWNTs-COOH reassembling restricts the movement of PA66 molecular chains, resulting in incomplete crystallization and decreased crystallinity. By comparing Table 2 with Table 4, the strength and crystallinity present a positive correlation, i.e., the higher the crystallinity, the higher the strength.

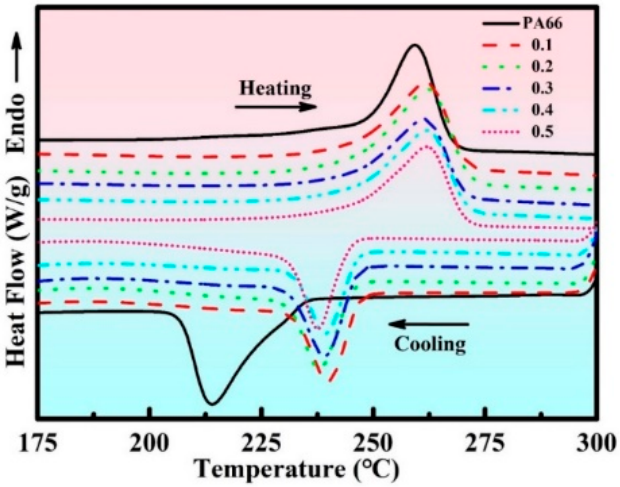

Figure 7. Differential scanning calorimeter (DSC) heating scans and cooling scans of the pure and the nanocomposite fibers.

Table 4. DSC melting and crystallization properties for the pure and the nanocomposite fibers.

Loading (wt %)	T_m (°C)	ΔH_m (J/g)	T_c (°C)	X_c (%)
0	259.6	64	232.0	33.0
0.1	261.8	64	239.8	33.0
0.2	262.0	65	239.1	33.5
0.3	262.2	75	239.2	38.8
0.4	261.5	60	237.9	31.4
0.5	262.0	61	237.6	31.6

The loss tangent (tan δ) of the pure PA66 fiber and the PA66/GO/MWNTs-COOH nanocomposite fibers with various GO/MWNTs-COOH loadings are shown in Figure 8. Due to the loss factor being positively correlated with the amorphous area of the fiber, as GO/MWNTs-COOH loading increases, from 0 to 0.3 wt %, the loss factor reduces from 0.104 to 0.058. It can also be seen that both the crystalline region and crystallinity of the fiber increase. Compared with T_g of the pure PA66 fiber (55.3 °C), T_g of 0.3 wt % GO/MWNTs-COOH nanocomposite fibers rises, reflected from the loss tangent peaks of the nanocomposite fibers shifting toward high temperature, increasing to 62.7 °C. T_g of nanocomposite fibers is enhanced due to GO/MWNTs-COOH with strong affinity dispersed evenly within the PA66 matrix, limiting polymer segmental motion and reducing the free volume.

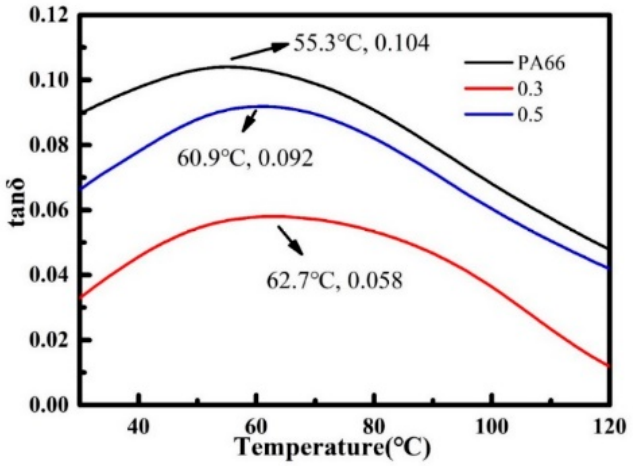

Figure 8. Tan δ versus temperature for the pure and the nanocomposite fibers with various GO/MWNTs-COOH loadings.

Figure 9 shows XRD patterns of pure PA66 and the PA66/GO/MWNTs-COOH nanocomposite fibers. PA66 is a polycrystalline polymer with α and β crystal shapes. The α-PA66 (100) (including β-PA66), (010), and (110) crystal surface diffraction peaks can be demarcated at diffraction angles 20.4° and 23.4°. The relative peak height of the (100), (010), and (110) peaks reduce with increased GO/MWNTs-COOH loading. This phenomenon is because crystals tend to grow along the (010) and (110) crystal surfaces when GO/MWNTs-COOH are added to PA66. According to Scherrer's equation, the grain size of the pure PA66 and the composite fiber can be obtained, as shown in Table 5. It shows that the grain size of the (100) crystal surface of the composite fiber is less than that of PA66, and those of the (010) and (110) crystal surfaces of the composite fiber are more than that of PA66. This explains why the degree of crystallization is increased, as it is caused by the action of heterogeneous nucleation of GO/MWNTs-COOH in the PA66 crystallization process, facilitating crystal growth along the (010) and (110) crystal surfaces.

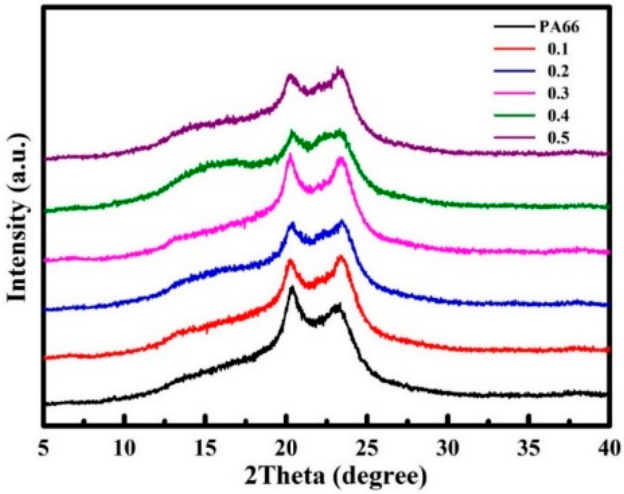

Figure 9. XRD patterns of the pure and the nanocomposite fibers.

Table 5. XRD data of the pure and the nanocomposite fibers.

Loading (wt %)	2θ (°)		*FWHM*		*D100* (nm)	*D010* (nm)
	α1	α2	α1	α2		
0	20.40	23.40	0.666	0.997	12.0	8.1
0.1	20.26	23.40	0.691	0.878	11.6	9.1
0.2	20.34	23.50	0.720	0.844	11.1	9.5
0.3	20.24	23.44	0.746	0.863	10.7	9.3
0.4	20.48	23.40	0.730	0.814	10.9	9.9
0.5	20.41	23.38	0.720	0.860	11.1	9.3

4. Conclusions

The physical, mechanical, and thermal properties of melt-spun PA66/GO/MWNTs-COOH nanocomposite fibers fabricated by using styrene–maleic anhydride copolymer treatment and solid-state shear milling were improved. MWNTs-COOH integrated into the layers of GO and dispersed uniformly in the PA66 matrix, and interfacial adhesions between GO/MWNTs-COOH and the PA66 was improved under the 3D forces exerted by the S3M. The mechanical properties of the S3M-treated nanocomposite fibers are better than that of the pure, non-S3M-treated fibers. In particular, the tensile strength and Young's modulus of the S3M-treated nanocomposite fibers with a 0.3 wt % GO/MWNTs-COOH loading reach up to 979 MPa and 6.37 GPa, respectively. In addition, the effect of S3M process on the crystallization and thermal properties of nanocomposite fibers is remarkable, leading to an increase of the thermal stability of the S3M-treated fibers with 0.3 wt % GO/MWNTs-COOH loading of 5.7 °C.

The utilization of SMA-treated GO/MWNTs-COOH, the S3M process, melt spinning, and the two-step drawing process all provide a facile and cost-effective method of the direct use of GO/MWNTs-COOH for the large-scale fabrication of nanocomposite fibers with excellent thermal properties and enhanced mechanical properties, which can be widely used at the industrial scale.

Author Contributions: Conceptualization, X.G. and X.Z.; Investigation, W.Y. and X.Z.; Supervision, Z.Z. and H.L.; Writing—original draft, X.G.; Writing—review & editing, X.Z.

Acknowledgments: This work was supported by the National Key Research and Development Program of China (grant number 2016YFB0303000) and the New Materials Research Key Program of Tianjin (grant number 16ZXCLGX00090).

Conflicts of Interest: The authors declare no conflict of interest.

References

1. Bellenger, V.; Tcharkhtchi, A.; Castaing, P. Thermal and mechanical fatigue of a PA66/glass fibers composite material. *Int. J. Fatigue* **2006**, *28*, 1348–1352. [CrossRef]
2. Jin, J.; Zhang, L.; Chen, W.; Li, C.Z. Synthesis of glass fiber-multiwall carbon nanotube hybrid structures for high-performance conductive composites. *Polym. Compos.* **2013**, *34*, 1313–1320. [CrossRef]
3. Chang, Q.X.; Zhao, H.J.; He, R.Q. The addition of clay on the mechanical properties of surface-treated CF-filled PA66 composites. *Surf. Interface Anal.* **2017**, *49*, 837–842. [CrossRef]
4. Meng, Q.J.; Wang, Z.M.; Zhang, X.X.; Wang, X.C.; Bai, S.H. Fabrication and properties of polyamide-6, 6-functionalized carboxylic multi-walled carbon nanotube composite fibers. *High Perform. Polym.* **2010**, *22*, 848–862. [CrossRef]
5. Zhang, X.X.; Meng, Q.J.; Wang, X.C.; Bai, S.H. Poly (adipic acid-hexamethylene diamine)-functionalized multi-walled carbon nanotube nanocomposites. *J. Mater. Sci.* **2011**, *46*, 923–930. [CrossRef]
6. Tran, T.Q.; Fan, Z.; Mikhalchan, A.; Liu, P.; Duong, H.M. Post-treatments for multifunctional property enhancement of carbon nanotube fibers from the floating catalyst method. *ACS Appl. Mater. Interfaces* **2016**, *8*, 7948–7956. [CrossRef] [PubMed]
7. Kim, Y.K.; Le, T.H.; Kim, S.; Park, G.S.; Yang, K.S.; Yoon, H.S. Single-walled carbon nanotube-in-binary-polymer nanofiber structures and their use as carbon precursors for electrochemical applications. *J. Phys. Chem. C* **2018**, *122*, 4189–4198. [CrossRef]
8. Chen, T.; Wang, Y.Z.; Liu, H.H.; Zhang, X.X. Melt-spinning of carboxylated MWNTs reinforced polyamide 6 fibers with solid mixing nanocomposites. *Polym. Compos.* **2018**, *39*, 4298–4309. [CrossRef]
9. Kim, J.W.; Oh, J.W.; Lee, K.Y.; Jung, I.; Park, M. Dispersion of graphene-based nanocarbon fillers in polyamide 66 by dry processing and its effect on mechanical properties. *Compos. Part B* **2017**, *114*, 445–456. [CrossRef]
10. Vijayaraghavan, V.; Zhang, L. Tensile and interfacial loading characteristics of boron Nitride-Carbon nanosheet reinforced polymer nanocomposites. *Polymers* **2019**, *11*, 1075. [CrossRef]
11. Nezhad, H.; Thakur, V. Effect of morphological changes due to increasing carbon nanoparticles content on the quasi-static mechanical response of epoxy resin. *Polymers* **2018**, *10*, 1106. [CrossRef] [PubMed]
12. Hasija, V.; Raizada, P.; Sudhaik, A.; Sharma, K.; Kumar, A.; Singh, P.; Jonnalagadda, S.B.; Thakur, V.K. Recent advances in noble metal free doped graphitic carbon nitride based nanohybrids for photocatalysis of organic contaminants in water: A review. *Appl. Mater. Today* **2019**, *15*, 494–524. [CrossRef]
13. Sharma, S.; Dutta, V.; Singh, P.; Raizada, P.; Rahmani-Sani, A.; Hosseini-Bandegharaei, A.; Thakur, V.K. Carbon quantum dot supported semiconductor photocatalysts for efficient degradation of organic pollutants in water: A review. *J. Clean. Prod.* **2019**, *228*, 755–769. [CrossRef]
14. Muhulet, A.; Miculescu, F.; Voicu, S.I.; Schütt, F.; Thakur, V.K.; Mishra, Y.K. Fundamentals and scopes of doped carbon nanotubes towards energy and biosensing applications. *Mater. Today Energy* **2018**, *9*, 154–186. [CrossRef]
15. Zhu, Y.; Higginbotham, A.L.; Tour, J.M. Covalent functionalization of surfactant-wrapped graphene nanoribbons. *Chem. Mater.* **2009**, *21*, 5284–5291. [CrossRef]

16. Kuila, T.; Bose, S.; Mishra, A.K.; Khanra, P.; Kim, N.H.; Lee, J.H. Chemical functionalization of graphene and its applications. *Prog. Mater Sci.* **2012**, *57*, 1061–1105. [CrossRef]
17. Layek, R.K.; Nandi, A.K. A review on synthesis and properties of polymer functionalized graphene. *Polymer* **2013**, *54*, 5087–5103. [CrossRef]
18. Wu, C.K.; Wang, G.J.; Dai, J.F. Controlled functionalization of graphene oxide through surface modification with acetone. *J. Mater. Sci.* **2013**, *48*, 3436–3442. [CrossRef]
19. Kinloch, I.A.; Suhr, J.; Lou, J.; Young, R.J.; Ajayan, P.M. Composites with carbon nanotubes and graphene: An outlook. *Science* **2018**, *362*, 547–553. [CrossRef]
20. Ren, Y.; Fu, Y.Q.; Liao, K.; Li, F.; Cheng, H.M. Fatigue failure mechanisms of single-walled carbon nanotube ropes embedded in epoxy. *Appl. Phys. Lett.* **2004**, *84*, 2811–2813. [CrossRef]
21. Wang, Z.M.; Zhang, X.X.; Wang, X.C.; Bai, S.H.; Qiao, Z.J. Preparation and properties of melt-blended carboxyl multi-walled carbon nanotubes/PA66 composite fibers. *Acta Mater. Compos. Sin.* **2011**, *8*, 16–21. [CrossRef]
22. Mahmood, N.; Islam, M.; Hameed, A.; Saeed, S.; Khan, A.N. Polyamide-6-based composites reinforced with pristine or functionalized multi-walled carbon nanotubes produced using melt extrusion technique. *J. Compos. Mater.* **2014**, *48*, 1197–1207. [CrossRef]
23. Wang, Z.M.; Bai, S.H.; Zhang, X.X.; Wang, X.C. Preparation and characterization of carboxylic multi-walled carbon nanotubes/PA66 composite by solution mixing process. *Acta Mater. Compos. Sin.* **2010**, *27*, 12–17. [CrossRef]
24. Deng, Z.; Yu, H.J.; Wang, L.; Zhai, X.T. A novel ferrocene-containing polymer based dispersant for noncovalent dispersion of multi-walled carbon nanotubes in chloroform. *J. Organomet. Chem.* **2015**, *791*, 274–278. [CrossRef]
25. Loyta, M.; Hernandez, Y.; King, P.J.; Smith, R.J.; Nicolosi, V.; Karlsson, L.S. Liquid phase production of graphene by exfoliation of graphite in surfactant/water solutions. *J. Am. Chem. Soc.* **2009**, *131*, 3611–3620. [CrossRef] [PubMed]
26. Wakabayashi, K.; Brunner, P.J.; Masuda, J.; Hewlett, S.A.; Torkelson, J.M. Polypropylene-graphite nanocomposites made by solid-state shear pulverization: Effects of significantly exfoliated, unmodified graphite content on physical. mechanical and electrical properties. *Polymer* **2010**, *51*, 5525–5531. [CrossRef]
27. Jiang, X.; Drzal, L.T. Reduction in percolation threshold of injection molded high-density polyethylene/exfoliated graphene nanoplatelets composites by solid state ball milling and solid-state shear pulverization. *J. Appl. Polym. Sci.* **2012**, *124*, 525–535. [CrossRef]
28. Shao, W.; Wang, Q.; Wang, F.; Chen, Y. Polyamide-6/natural clay mineral nanocomposites prepared by solid-state shear milling using pan-mill equipment. *J. Polym. Sci. Part B Polym. Phys.* **2006**, *44*, 249–255. [CrossRef]
29. Shao, W.; Wang, Q.; Wang, F.; Chen, Y. The cutting of multi-walled carbon nanotubes and their strong interfacial interaction with polyamide 6 in the solid state. *Carbon* **2006**, *44*, 2708–2714. [CrossRef]
30. Zhou, L.; Liu, H.; Zhang, X. Graphene and carbon nanotubes for the synergistic reinforcement of polyamide 6 fibers. *J. Mater. Sci.* **2015**, *50*, 2797–2805. [CrossRef]
31. Yan, D.; Yang, G. A novel approach of in situ grafting polyamide 6 to the surface of multi-walled carbon nanotubes. *Mater. Lett.* **2009**, *63*, 298–300. [CrossRef]
32. He, Z.X.; Zhang, B.Q.; Zhang, H.B.; Zhi, X.; Hu, Q.H.; Gui, C.X.; Yu, Z.Z. Improved rheological and electrical properties of graphene/polystyrene nanocomposites modified with styrene maleic anhydride copolymer. *Compos. Sci. Technol.* **2014**, *102*, 176–182. [CrossRef]
33. Shah, D.; Maiti, P.; Jiang, D.D.; Batt, C.A.; Giannelis, E.P. Effect of nanoparticle mobility on toughness of polymer nanocomposites. *Adv. Mater.* **2005**, *17*, 525–528. [CrossRef]
34. Meng, H.; Sui, G.X.; Fang, P.F.; Yang, R. Effects of acid-and diamine-modified MWNTs on the mechanical properties and crystallization behavior of polyamide 6. *Polymer* **2008**, *49*, 610–620. [CrossRef]

35. Chen, T.; Liu, H.H.; Wang, X.C.; Zhang, H.; Zhang, X.X. Properties and fabrication of PA66/surface-modified multi-walled nanotubes composite fibers by ball milling and melt-spinning. *Polymers* **2018**, *10*, 547. [CrossRef] [PubMed]
36. Fang, M.; Pan, D.D.; Gao, X.; Yao, M.J. Extension-induced mechanical reinforcement in melt-spun fibers of polyamide 66/multiwalled carbon nanotube composites. *Polym. Int.* **2011**, *60*, 1646–1654. [CrossRef]